Electron loss from fast heavy ions: Target-scaling dependence

R. D. DuBois,[1] A. C. F. Santos,[2] G. M. Sigaud,[3] and E. C. Montenegro[2]

[1]*Department of Physics, Missouri University of Science and Technology, Rolla, Missouri 65409, USA*

[2]*Instituto de Física, UFRJ, Caixa Postal 68528 Rio de Janeiro, BR-21941-972 RJ, Brazil*

[3]*Departamento de Física, Pontifícia Universidade Católica do Rio de Janeiro, Caixa Postal 38071, Rio de Janeiro, BR-22452-970 RJ, Brazil*

(Received 13 April 2011; published 4 August 2011)

The target dependence for projectile electron loss is investigated using experimental data taken from the literature. Impact energies range from a few tens of eV/u to tens of MeV/u. For energies less than several MeV/u, the target dependences are shown to be very similar, independent of projectile species and charge state. Overall, however, with increasing impact energy the cross-section dependence on the target nuclear charge systematically increases. It is shown that none of the existing cross-section target scaling models reproduce these features. A model, based on Born scaling and including both the antiscreening and screening contributions to projectile electron loss, is developed. With the inclusion of relativistic effects, which increase the contribution from both channels at high energies, and "target saturation" effects, which reduce the contribution from the screening term for heavy targets and lower impact energies, this model describes quite reasonably all available experimental data. A simple scaling formula that reproduces the measured atomic number and impact velocity dependences is provided. This formula is applicable for projectile electron loss in collisions with either atomic or molecular targets and for impact energies ranging from a few to tens of MeV/u.

DOI: 10.1103/PhysRevA.84.022702 PACS number(s): 34.50.Fa, 34.50.Bw

I. INTRODUCTION

Fast ions traversing any medium, e.g., a dilute gas, condensed matter, biological material, or a plasma, undergo inelastic interactions with the atomic and molecular components of the medium. This transfers energy from the ion to the media. As a result, the media is altered both chemically and physically, and the kinetic energy of the ion is reduced. Also, in particular at higher impact energies, the projectile can be ionized. The current work was initiated to address a long-standing question as to how projectile ionization scales for different targets. Another long-standing question has also been addressed, namely, the velocity dependence in the intermediate- to high-energy regime for electron-loss processes.

Projectile ionization is also referred to as projectile stripping or electron loss. For interactions with atomic targets, it has the form

$$P^{q+} + T \rightarrow P^{(q+n)+} + T^{i+} + (n+i)e^{-}. \qquad (1)$$

Here P represents the fast ion (the projectile) with charge q, T is the target atom, and n and i are the number of projectile and target electrons that are liberated during the collision, respectively. Note that projectile ionization requires $n \geqslant 1$, while the target can either be simultaneously ionized or remain in its initial state. Hence, $i \geqslant 0$. Equation (1) also applies for neutral ($q = 0$) and negative projectiles ($q < 0$). For interactions with molecular targets, Eq. (1) must be altered to include target fragmentation into charged and uncharged components.

Numerous electron-loss studies have been performed over the decades due to its fundamental and applied importance. From a basic atomic physics viewpoint, they are useful for investigating and understanding atomic processes and interactions. For example, they have an advantage over target ionization studies in that few- to many-electron systems can be systematically studied simply by altering the projectile nuclear, Z_P, and total, q, charges. They can be used to investigate the passive and active participation of bound target electrons by comparing electron-loss data obtained using different targets or by using data obtained for the same target but where simultaneous and independent ionization of the target and projectile are compared.

Electron-loss studies have also been performed for applied purposes. One major reason is associated with radiation damage of materials and/or of biological tissues by high-energy particles. Another is with regard to the creation, acceleration, transport, and storage of ions for research purposes. For example, electron loss occurring when high-energy beams interact with background gases within beamlines or storage rings has serious detrimental effects. These include loss of beam luminosity (due to scattering), decreased storage times (due to losses at bending magnets or focusing elements because of altered charge states or degraded energies), and possible erosion, heating, or vacuum loading in the accelerator and storage rings (due to interactions with the vacuum walls, lenses, etc. by the lost beam components). Any lost beam components can lead to localized heating of surfaces. This desorbs gases or atoms from the surfaces, which further degrades the vacuum, which increases the loss processes, etc. In the worst case, an avalanche effect takes place resulting in complete loss of the beam. Increased radiation levels during operation in addition to nuclear activation of beamline components are also major concerns. All of these are crucial technical problems at high-energy accelerator laboratories, e.g., at GSI, Brookhaven, CERN, Dubna, etc., where considerable effort and expense are being devoted in order to predict and circumvent such problems [1–3].

As an example, a goal of the new Facility for Antiproton and Ion Research (FAIR) at the GSI Helmholzzentrum für Schwerionenforschung in Darmstadt, Germany, is to produce

intense beams of high-energy heavy ions [4]. To obtain high beam intensities and densities, the lowest possible charge-state ions must be used in order to reduce the space charge. For such ions traveling with MeV/u to GeV/u velocities, electron loss is the dominant mechanism. Thus, to avoid or to minimize problems, information about total loss probabilities, and information about what charge states are produced and with what relative probabilities, are needed for a broad range of systems and energies. The systems include interactions with few-electron targets such as H_2 and He, i.e., the primary components found in high vacuum environments, plus interactions with many-electron targets such as N_2, CO, CO_2, H_2O, etc., which occur as lesser components in the vacuum or which can be desorbed from surfaces. Even though they may be far less abundant, interactions with heavier gases are especially important because they have large cross sections. Hence, locally or on average, they can contribute significantly to the total beam losses. In addition, interactions with heavier atoms and molecules are primarily responsible for multiple-electron loss from the ion. This is important because ions which have suffered multiple, as opposed to single, electron loss will follow different trajectories and will impact surfaces at different locations depending upon their charge. For these reasons, numerous experimental and theoretical studies of electron loss have been performed throughout the years.

Calculating or measuring all possible systems and energies can be avoided if scaling rules can be established. However, as will be shown, the different scaling models which have been suggested do not account for the similarities and trends found in the experimental data. Here, we present a method of determining the number of target electrons which actively and passively contribute to projectile electron loss. Our method includes relativistic and "target saturation" effects which, respectively, increase the number of active and passive target electrons at high energies and reduce the number of passive electrons for heavy targets and lower energies. A simple scaling formula that reproduces observed experimental features for a wide variety of systems and impact energies is provided.

II. TARGET SCALING: EXPERIMENTAL OVERVIEW

Electron-loss cross sections have been measured for atomic targets ranging from helium to xenon [5–14]. These studies have shown that for lighter targets, typically meaning for $Z_T < 10$, where Z_T is the target nuclear charge, the cross sections increase rapidly, e.g., approximately as Z_T^n, where $n \sim 1.4$–1.7. But, for heavier targets the cross sections increase more slowly and appear to saturate in some cases. Examples of some of these data are shown in Fig. 1 where, for comparison purposes, the target dependence for each ion has been normalized to unity at $Z_T = 10$. Because of this normalization and the different target dependences, the curves for different energies intersect and cross at $Z_T = 10$. The data in Fig. 1 cover an extremely broad range of energies, e.g., over six orders of magnitude with the highest velocities being approximately a quarter of the speed of light. They also cover a wide range of ion species, e.g., singly charged ions ranging from He^+ to Kr^+, one-electron ions such as He^+ and N^{6+}, low- and medium-charge state, and heavy ions such as Ar^{6+}, Ar^{8+}, Fe^{4+}, Xe^{18+}, U^{4+}, U^{6+}, U^{10+}, and Pb^{54+}.

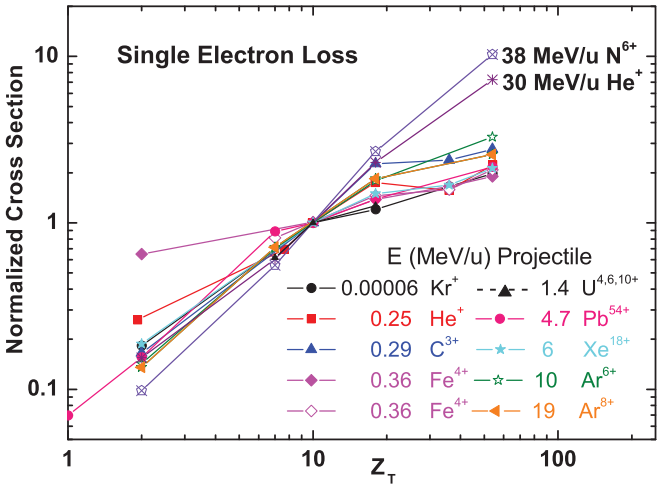

FIG. 1. (Color online) Single-electron-loss cross sections measured for various ions and ion energies as a function of the target atomic number, Z_T, normalized to unity at $Z_T = 10$. Because of this normalization and the different target dependences, the curves for different energies intersect and cross at $Z_T = 10$. The experimental data are from the following sources: Kr^+, Ref. [12]; 0.25 MeV/u He^+, Ref. [6]; C^{3+}, Ref. [7]; Fe^{4+}, Refs. [5,13]; U^{4+}, U^{6+}, and U^{10+}, Ref. [11]; Pb^{54+}, Ref. [14]; Xe^{18+}, Ref. [8]; Ar^{6+} and Ar^{8+}, 30 MeV/u He^+ and N^{6+}, Refs. [9,10].

As seen, in spite of the vast differences in velocities and ion species, the normalized electron-loss data for energies between 60 eV/u and 19 MeV/u have very similar target dependences which agree in shape within approximately a factor of 2. These dependences are in sharp contrast to the much steeper dependences and no apparent change in slope between the "light" and "heavy" target regime that is observed for the two highest energies.

A closer look, however, shows that there is a general trend toward steeper and steeper slopes with increasing energy. It should be noted that although the comparisons shown are made using single-electron-loss data, similar comparisons using total (the sum of all single- and multiple-loss cross sections) and weighted (the sum of the individual cross sections multiplied by the number of projectile electrons lost in each case) electron-loss cross-section data yield similar features. The only difference is that in going from single loss to total loss to weighted loss, the spread in the data for $Z_T < 10$ significantly decreases.

III. OVERVIEW OF THEORETICAL MODELS AND COMPARISON WITH EXPERIMENT

Over the years, numerous theoretical models for calculating electron loss and for describing how electron loss scales as a function of impact velocity or target have been introduced. In this section we briefly outline many of these methods with emphasis on what scaling features they predict.

One of the first models was introduced in 1948 by Bohr who used the Thomas-Fermi model to estimate the screened Coulomb potential between two approaching atoms [15].

He predicted that in collisions of heavy systems the cross section for single-electron loss should scale as $(Z_P{}^{1/3} + Z_T{}^{1/3})^2$, where Z_P is the projectile nuclear charge. A few years later Firsov [16] numerically derived the interatomic potentials of two colliding Thomas-Fermi atoms and fitted these potentials using the Thomas-Fermi screening length. He obtained a slightly different scaling, namely, $(Z_P{}^{1/3} + Z_T{}^{1/3})^{2/3}$. Several decades later, Alton *et al.* [5] modified the Bohr formula slightly by multiplying by the number of target electrons in the outermost subshell and dividing by their ionization potential. With this modification, better agreement with the experimental measurements as a function of Z_T was found.

Bates and Griffing outlined the basic method for performing quantitative calculations of electron loss many years ago [17]. They showed that two interaction channels, one involving the interaction of a partially screened target nucleus with the projectile electron, the other involving a direct interaction between a target and a projectile electron, must be considered. The first mechanism—where the target electrons remain in their initial state and have a passive role of shielding the nuclear charge—decreases the ionization amplitude with respect to that from an unscreened nucleus. It has been referred to as the screening, the *e-n*, or the elastic channel. The second mechanism—where the target electrons actively participate in ionization of the projectile—has been called the antiscreening (reflecting the fact that it increases the electron-loss cross section), the *e-e*, or the inelastic channel [18–20].

Using the Born approximation, Bates and Griffing showed that these channels contribute to the differential cross sections for projectile ionization by neutral targets as follows:

$$\text{screening}: \quad d^2\sigma(\varepsilon) = \int_{q\ \min} A(\varepsilon,q)[|Z_T - Z_T F(q)|^2]\,dq \tag{2}$$

and

$$\text{antiscreening}: \quad d^2\sigma(\varepsilon) = \int_{q'\ \min} A(\varepsilon,q) \times [Z_T - Z_T|F(q)|^2]\,dq, \tag{3}$$

where $F(q)$ is the target electron form factor as a function of the momentum transfer, q, and $A(\varepsilon,q)$ contains information about the projectile. For the screening channel, Eq. (2), the bracketed term represents the target nuclear charge, Z_T, partially screened by some of its bound electrons, and is referred to as the effective target nuclear charge, $Z_{T\text{eff}}$. Thus, the screening cross section scales as $Z^2_{T\text{eff}}$. In contrast, for the antiscreening channel, Eq. (3), the term within brackets represents the number of target electrons which interact directly with those of the projectile. We will refer to this as $N_{T\text{eff}}$, the effective number of target electrons. The antiscreening cross section scales linearly with $N_{T\text{eff}}$. Since the values of $F(q)$ lie between 0 and 1, both $Z_{T\text{eff}}$ and $N_{T\text{eff}}$ can vary from Z_T to 0. Additional details can be found in [21].

One important point to note is that the calculations of *e-n* and *e-e* channels in Eqs. (2) and (3) have different integration lower limits for the momentum transfer. For the *e-n* channel only the projectile electron is ionized, while for the *e-e* channel the momentum transfer is required to remove electrons from both the projectile and the target. For few-electron projectiles and energies well above threshold, these differences are unimportant and the Born model predicts that the electron-loss cross sections will scale as $Z^2_{T\text{eff}} + N_{T\text{eff}}$. For many-electron targets, inner shell electrons must also be included and these electrons are much more tightly bound. Thus, Eqs. (2) and (3) have to be applied shell by shell which makes the values for $Z_{T\text{eff}}$ and $N_{T\text{eff}}$ depend on the impact energy. This complicates the calculations or requires information about "average" values for $Z_{T\text{eff}}$ and $N_{T\text{eff}}$.

Another complicating issue regarding heavy targets is the breakdown of the perturbative treatment, which is the basis of Eqs. (2) and (3), due to the large field of the target nucleus in collisions with small impact parameters. One approach to include this was introduced by Voitkiv, Sigaud, and Montenegro [22]. They used the sudden approximation and accounted for the nonperturbative character of the collision and the possibility of multielectron transitions in the target atom to calculate electron loss from He^+ projectiles in collisions with heavy targets. They determined the cross sections for the screening contribution for He^+ ions in noble gases and were able to describe rather well the saturation of this contribution as the atomic number of the target increases.

In contrast with the screening, the antiscreening mode can be well treated using perturbative approaches. Following the ideas of Anholt [18], Montenegro and co-workers [23,24] showed that the antiscreening contribution, within the impulse approximation [25], was equal to the electron-impact ionization cross section times the average number of active target electrons, e.g., $\sigma_{\text{anti}} = \langle n\rangle\sigma_e$. Thus, from measured antiscreening cross sections, i.e., cross sections where projectile and target ionization are measured in coincidence, and calculated or measured electron-impact cross sections, the average number of active target electrons, i.e., $\langle n\rangle$, could be determined.

More recently, Santos *et al.* [7,26] further explored these concepts and used C^{3+} and He^+ data to determine the ratio $\sigma_{\text{anti}}/\sigma_e$, which combined with the impulse approximation, enabled them to estimate the average number of active target electrons for the antiscreening mode. This was done as a function of collision energy and fitted to

$$\langle n\rangle_E = f(E)\langle n_\infty\rangle, \tag{4}$$

where $\langle n_\infty\rangle$ is the value of the average number of active target electrons at a very high impact energy and $f(E)$ is a function of the collision energy, E. Based on the impulse approximation, estimates for $\langle n_\infty\rangle$ were obtained which included contributions from all target subshells, providing the following values: 1.4 for He, 5 for N, 5.8 for Ne, 7.8 for Ar, 12.4 for Kr, and 15.1 for Xe. However, this method yielded a result where the active number of electrons for the antiscreening channel decreased with increasing impact energy. This is counterintuitive to the idea that more bound electrons become energetically accessible at higher energies, a point that was addressed in their recent He^+ paper [26].

If we limit ourselves to few-electron targets or where only a single shell is involved, reasonable values for the screening and antiscreening cross sections result. For example,

Meyerhof *et al.* [27] used the PWBA (plane wave Born approximation) to calculate electron loss from few-electron ions such as He^+ and O^{7+} colliding with molecular hydrogen. They found that even though the binding energies of the ionized electrons are quite different for the two projectiles, the antiscreening and screening processes have the same relative magnitudes and energy dependences. Several studies by Montenegro and co-workers [6,7,28–30] also used the PWBA to calculate electron loss from few-electron ions such as He^+, C^{3+}, and O^{5+}. Of particular relevance to the present work is that these studies implied that the scaling for the screening channel is influenced by saturation effects occurring for heavy targets, i.e., for large Z_T [29,31],.

Concomitantly, with these and other studies which mainly focused on the understanding of the dynamical details of the electron-loss processes, other studies concentrated on cross-section scaling. Shevelko developed the LOSS-R code [32,33] which used the PWBA to calculate single-electron-removal processes induced by protons and electrons. These were then scaled to simulate ionization by the nucleus and bound electrons of various atomic and molecular targets. For electron loss from Pb-like ions [34] the cross sections were found to scale as $(Z_T/I_P)^{1.4}$ and the energy to scale with I_P, where I_P is the projectile ionization potential. This code was further developed and modified into the DEPOSIT code which was based upon a semiclassical model [33].

In 1985, Kaneko used a unitarized impact-parameter method to calculate electron loss and excitation from He^+ colliding with various atoms [35]. With regard to the target dependence, he found that the cross sections scale roughly as $Z_T{}^{1.3}$ for $Z_T < 10$. For $Z_T > 10$, the scaling is slower, e.g., with powers decreasing from 0.39 to 0.17 as the impact velocity increases from 0.1 to 0.9 MeV/u.

Extensive calculations of single- and multiple-electron loss for a variety of systems were performed by Olson who used an *n*-body classical trajectory Monte Carlo (nCTMC) method [8,36–39]. This theory includes multiple-electron removal processes and has been applied to many types of atomic interactions between many-electron projectiles and targets. However, these studies primarily concentrated on energy and charge-state dependences for specific systems, and target-scaling properties were not explicitly discussed.

Many models and calculations appearing in the literature were applied to specific cases and are not suitable to obtain general scalings valid for a broad range of targets and projectile velocities. Therefore, in Fig. 2 we compare available experimental data with theories which have clearly defined predictions for the target-scaling dependences. The experimental data (normalized to unity at $Z_T = 10$) are the same as in Fig. 1. Here 38 MeV/u N^{6+} are the solid black circles, 30 MeV/u He^+ are the solid gray triangles, and the open red stars are average values calculated for all energies smaller than 10 MeV/u. The solid line, Born Z_T, is a Born dependence which assumes stripping by the full nuclear charge and all of the bound electrons, e.g., $Z_T{}^2 + Z_T$. It can be seen that this scaling yields a much steeper dependence than is observed for even the highest-energy data and yields no change in slope such as that observed in the lower-energy data. Better agreement to the high-energy data is obtained if, instead of

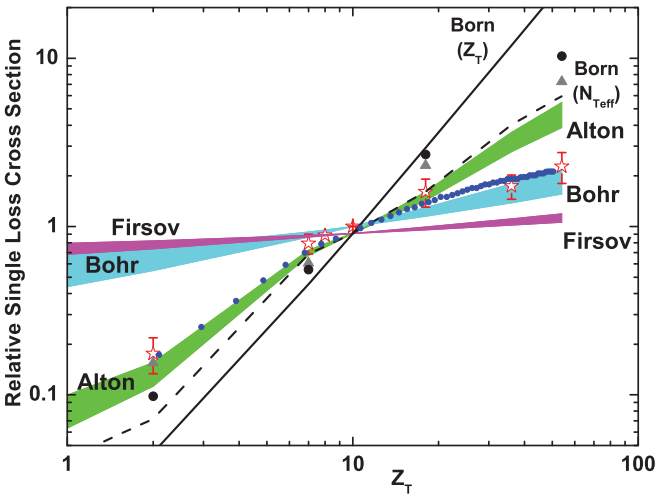

FIG. 2. (Color online) Single-electron-loss cross sections compared to various theoretical models as a function of the target atomic number, Z_T, normalized to unity at $Z_T = 10$. The experimental data are the same as in Fig. 1. Here, the filled circles and triangles are the 38 and 30 MeV/u data, respectively, and the open stars represent average values calculated for energies less than 10 MeV/u. For explanations of the theoretical calculations, see text.

using the full nuclear and bound electron charges, we use a simple assumption that at a particular impact energy there is an average impact parameter outside which all electrons contribute to the antiscreening channel and inside which all electrons screen the nuclear charge. Under this assumption, the overall scaling becomes $N_{T\text{eff}}^2 + N_{T\text{eff}}$, shown by the dashed curve, Born $N_{T\text{eff}}$. For the effective number of electrons, $N_{T\text{eff}}$, we used the values averaged for all target subshells suggested by Santos *et al.* [7] that were listed above. This improves the Born model somewhat at the higher energies but predicts cross sections that are much too large for heavy targets and lower energies.

The blue band shows Bohr scaling [15], namely, $(Z_P{}^{1/3} + Z_T{}^{1/3})^2$, which agrees reasonably well with the low-energy data for heavy targets but drastically overestimates the relative cross sections for light targets. The green band represents the Alton model [5] without the division by the ionization potentials. With this division, the slope in the low Z_T region will decrease with relatively little change in the higher Z_T region. Thus, although the Alton model yields much better agreement for lighter targets, it produces poorer agreement for heavy targets. The scaling suggested by Firsov [16], e.g., $(Z_P{}^{1/3} + Z_T{}^{1/3})^{2/3}$, the magenta band, has a very flat target dependence and agrees poorly with experiment. Since these models all have projectile, as well as target, nuclear charge dependences, the bands show limiting values obtained using $Z_P = 1$ and 92.

Although for ionization of 0.09 MeV/u He^+, the calculations of Kaneko [35] (the small blue filled circles) predict a target dependence that matches the low-energy data very well. However, with increasing velocity, this theory predicts that the target dependence should become flatter, whereas the available data indicate just the opposite. Thus, the apparently good agreement seen in Fig. 2 is coincidental.

IV. PRESENT WORK AND FINDINGS

The comparisons presented in the last section lead to the conclusion that none of these scaling rules are compatible with experiment over the entire range of energies and targets. In this section, a model is developed aiming to improve the agreement. The model is based on using the closure approximation, as outlined by Montenegro and Meyerhof [31], to obtain estimates for $Z_{T\text{eff}}$ and $N_{T\text{eff}}$. The screening and antiscreening cross sections can be written as [20,31]

$$\sigma_{\text{screen}} = \frac{8\pi}{\left(\frac{v}{v_0}\right)^2}\int_{q_0}^{\infty}\frac{dq}{q^3}|F_{sf}(q)|^2\left|Z_T - \langle\phi_0|\sum_i e^{i\vec{q}\cdot\vec{r}_i}|\phi_0\rangle\right|^2 \tag{5}$$

and

$$\sigma_{\text{anti}} = \frac{8\pi}{\left(\frac{v}{v_0}\right)^2}\sum_{n\neq 0}\int_{q_{\min}}^{\infty}\frac{dq}{q^3}|F_{sf}(q)|^2\left|\langle\phi_n|\sum_i e^{i\vec{q}\cdot\vec{r}_i}|\phi_0\rangle\right|^2. \tag{6}$$

Here, v_0 is the Bohr velocity, v is the projectile velocity, and q is the momentum transfer with $q_{\min} = q_0 + q_n$ which includes both target and projectile ionization and excitation. Values for q_0 and q_n are given by $q_0 = (\Delta E)_{\text{projectile}}/\hbar v$ and $q_n = (\Delta E)_{\text{target}}/\hbar v$. Thus, for the screening channel with the target remaining in its initial state, $q_n = 0$, $q_{\min} = q_0$. φ_0 and φ_n are the initial and final target wave functions, respectively. $F_{sf}(q)$ is defined as $F_{sf}(q) = \langle\phi_f|e^{i\vec{q}\cdot\vec{r}}|\phi_s\rangle$, where φ_s and φ_f are the initial and final projectile wave functions, respectively.

Recalling that $F_0(q) = \langle\phi_0|\sum_i e^{i\vec{q}\cdot\vec{r}_i}|\phi_0\rangle$ is the form factor for the target initial state, the screening cross section can be written as

$$\sigma_{\text{screen}} = \frac{8\pi}{\left(\frac{v}{v_0}\right)^2}\int_{q_0}^{\infty}\frac{dq}{q^3}|F_{sf}(q)|^2|Z_T - F_0(q)|^2. \tag{7}$$

The term $|\langle\phi_n|\sum_i e^{i\vec{q}\cdot\vec{r}_i}|\phi_0\rangle|^2$ which appears in the antiscreening cross section, e.g., Eq. (5), can be approximated by

$$\left|\langle\phi_n|\sum_i e^{i\vec{q}\cdot\vec{r}_i}|\phi_0\rangle\right|^2 \cong \frac{|F_0(q)|^2}{Z_T}. \tag{8}$$

This is a reasonable approximation for the antiscreening as the major contribution for this channel comes from the equivalent electrons in the outermost shells.

Substituting Eq. (8) into Eq. (6), the antiscreening cross section becomes

$$\sigma_{\text{anti}} = \frac{8\pi}{\left(\frac{v}{v_0}\right)^2}\int_{q_0}^{\infty}\frac{dq}{q^3}|F_{sf}(q)|^2\left[Z_T - \frac{|F_0(q)|^2}{Z_T}\right]. \tag{9}$$

In Eqs. (7) and (9) we define the effective charges seen by the projectile electron to be

$$Z_{T\text{eff}} = Z_T - F_0(q) \quad \text{and} \quad N_{T\text{eff}} = Z_T - \frac{|F_0(q)|^2}{Z_T} \tag{10}$$

for the screening and antiscreening channels, respectively.

Within the impulse approximation, the antiscreening cross section can be written as [7,24–26]

$$\sigma_{\text{anti}} = \sum_{nl} N_{nl}\sigma_{if}\left(q_{\min}^{nl}\right). \tag{11}$$

Here N_{nl} is the number of electrons in the nl target subshell which actively participate in the antiscreening channel and

$$\sigma_{if}(q_{\min}) = \sigma_{\text{screen}} = \frac{8\pi}{\left(\frac{v}{v_0}\right)^2}\int_{q_{\min}}^{\infty}\frac{dq}{q^3}|F_{sf}(q)|^2 \tag{12}$$

is the PWBA cross section for ionization of the projectile by a pointlike particle of unit charge [24,25]. In Eq. (11), $q_{\min}^{nl}$ is the minimum momentum transfer for an electron occupying the nl subshell of the target [7,26].

Since outershell electrons of the target give the largest contribution to the antiscreening channel, the values of $q_{\min}^{nl}$ do not vary significantly for the nl target subshells which effectively contribute to the projectile loss. Thus, from the above equations,

$$\sigma_{\text{anti}} = N_{T\text{eff}}\sigma_{if}(q_{\min}), \quad \text{where} \quad N_{T\text{eff}} \cong \sum_{nl} N_{nl} = \langle n_0\rangle. \tag{13}$$

Here, $\langle n_0\rangle$ is the average number of active target electrons in the antiscreening channel as given by Santos *et al.* [7,26].

Finally, rewriting the right half of Eq. (10) as

$$F_0(q) \cong \sqrt{Z_T(Z_T - N_{T\text{eff}})}, \tag{14}$$

and combining it with the left half of Eq. (10) yields

$$Z_{T\text{ eff}} \cong Z_T\left[1 - \sqrt{1 - \frac{N_{T\text{eff}}}{Z_T}}\right]. \tag{15}$$

Thus, the number of active electrons participating in the antiscreening channel, i.e., those which interact directly with projectile electrons, $N_{T\text{eff}}$, is given by $\langle n_0\rangle$, while the number of electrons which participate indirectly by partially screening the target nuclear charge is given by

$$Z_T\sqrt{1 - \frac{N_{T\text{eff}}}{Z_T}}. \tag{16}$$

Equation (13) predicts that the number of target electrons that participate directly is $\langle n_0\rangle$, which defines $N_{T\text{eff}}$, while, from Eq. (15), the screened nuclear charge of the target, $Z_{T\text{eff}}$, is given by $Z_T[1 - \{1 - N_{T\text{eff}}/Z_T\}^{1/2}]$. Using the $\langle n_0\rangle$ values from Refs. [7] and [26] results in $Z_{T\text{eff}} \approx \frac{1}{2}N_{T\text{eff}}$.

However, this overlooks two details. First, at high impact velocities, one would expect that eventually all target electrons will actively participate in the ionization process and that their ability to screen a portion of the target nuclear charge will decrease. Thus, at high velocities, both $N_{T\text{eff}}$ and $Z_{T\text{eff}}$ should increase and ultimately approach the full nuclear charge. Second, the ionization probabilities must be less than unity. Since the screening probabilities scale as the square of effective target nuclear charge, this means that at low energies and heavy targets the $Z_{T\text{eff}}$ values predicted by Eq. (15) will be too large.

To model the increases in $N_{T\text{eff}}$ and $Z_{T\text{eff}}$ at high energies, the following scenario was used. Our method of determining these parameters assumed a standard Coulomb field from a point particle. However, relativistic effects increase the transverse electric field of a point charge by a factor of $1/\sqrt{1-(v/c)^2}$. This means that, with increasing velocity, relativistic effects will cause the field of the target electrons—in the projectile frame—to extend further and further. This

will enhance the role of distant collisions and "activate" more and more target electrons which were not participating in the projectile ionization at lower velocities. This activation of additional electrons should be approximately true for all impact parameters. To model this increase, we multiplied the number of "inactive" electrons by the increase in the field beyond that of a normal Coulomb field. This increase was added in an *ad hoc*, phenomenological way, to our original fixed values of $\langle n_0 \rangle$ to determine $N_{T\mathrm{eff}}$. Hence,

$$N_{T\mathrm{eff}} = \langle n_0 \rangle + A\{Z_T - \langle n_0 \rangle\}\left\{-1 + 1\Big/\sqrt{1-\left(\frac{v}{c}\right)^2}\right\}. \tag{17}$$

Here, $Z_T - \langle n_0 \rangle$ is the number of electrons which were previously considered to be inactive, and the final bracketed term incorporates the effect of the increase in the transverse field of the target electrons in the projectile frame. The quantity A is a free parameter which, by trial and error, was found to be approximately 10 in order to provide the best fit to the data. It must be noted that in applying this model, the maximum values for $N_{T\mathrm{eff}}$ and $Z_{T\mathrm{eff}}$ are limited to be Z_T. Whereas previous work considered relativistic effects to affect only the screening mode [40], our procedure includes relativistic effects in both screening and antiscreening modes through Eqs. (15) and (17).

To model the decreases required at low energies and avoid violating the constraint that the ionization probabilities cannot exceed unity, we followed the suggestion of Sant'Anna *et al.* [29]. They observed that the electron-loss cross section saturates as Z_T/v increases and that this was associated with the screening component of the cross section. Therefore we multiplied $Z_{T\mathrm{eff}}$ by $e^{-Z_{T\mathrm{eff}}/v\ (\mathrm{in\ a.u.})}$, where v is the impact velocity in atomic units. With this addition, extremely good agreement with experimental data was achieved for energies up to several MeV/u.

Summarizing, our "modified Born" model which is applicable for electron loss from any projectile colliding with any target predicts that the electron-loss cross sections will scale as

$$\sigma = \sigma_H[N_{T\mathrm{eff}} + (Z_{T\mathrm{eff}}e^{-Z_{T\mathrm{eff}}/v\ (\mathrm{in\ a.u.})})^2]. \tag{18}$$

Here σ is the projectile electron-loss cross section per target atom, σ_H is the cross section for stripping via interactions with atomic hydrogen, $N_{T\mathrm{eff}}$ and $Z_{T\mathrm{eff}}$ are determined using Eqs. (17) and (15), respectively. Values used for the various quantities were $A = 10$ (determined by trial and error);

$$\log_{10}(\langle n_0 \rangle) = -0.16 + 1.08\ \log_{10}(Z_T) - 0.177\ \log_{10}(Z_T)^2 \tag{19}$$

(determined from fitting a polynomial to the asymptotic values given in Ref. [26]); v in the exponential saturation term is the projectile velocity in atomic units; and, in all cases, relativistic values were used for the velocities. Z_T is the full nuclear charge of the target. For applying the above formula for molecular targets, the average nuclear charge for the molecule as obtained using the procedure outlined by Watson *et al.* [8] is used for Z_T. For example, for projectile ionization by a water molecule, $Z_T = 1(2/3) + 8(1/3) = 3.3$, i.e., the full nuclear charge of each component atom multiplied by the fractional number of total atoms that this atom represents.

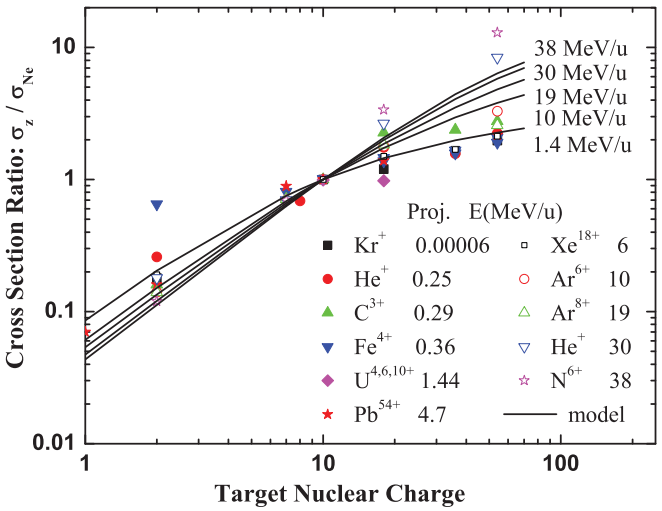

FIG. 3. (Color online) Normalized single-electron-loss cross sections as a function of target atomic number, Z_T, compared to the present model. Data are the same as in Fig. 1.

This scaling and these values imply that above approximately 80 MeV/u, both $N_{T\mathrm{eff}}$ and $Z_{T\mathrm{eff}}$ can exceed the full target nuclear charge. This occurs when $N_{T\mathrm{eff}} = Z_T$ in Eq. (17), i.e., for $v/c \sim 0.42$ when $A = 10$. Therefore, in applying this formula, both quantities were limited to their maximum values of Z_T for energies above ~80 MeV/u. Also, because $N_{T\mathrm{eff}}$ and $Z_{T\mathrm{eff}}$ are changing rather rapidly as they approach their limiting values, the scaling factors and scaled cross sections will have small changes in slope for energies near 80 MeV/u. These are artificial in nature. To avoid such features, in the following we have limited the maximum energy of our model to 70 MeV/u. As a final note, the scaling calculations become more amenable if v (in a.u.) is replaced by the collision energy in MeV/u divided by 0.025 in the saturation exponential and $(v/c)^2$ in Eq. (17) for $N_{T\mathrm{eff}}$ is replaced by twice the collision energy in MeV/u divided by 931.

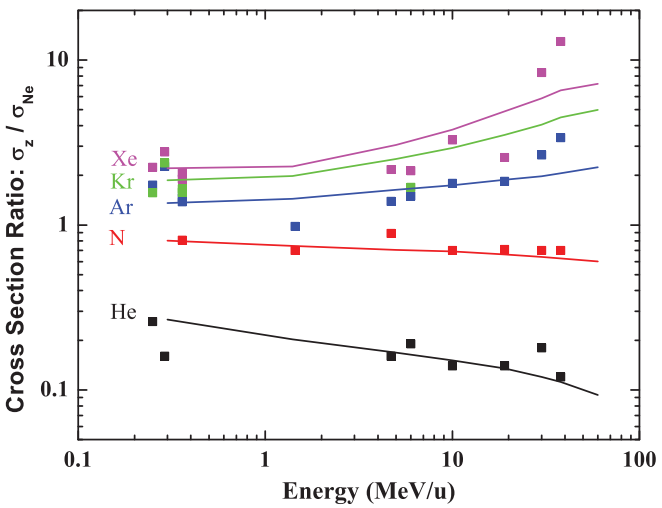

FIG. 4. (Color online) Normalized single-electron-loss cross sections as a function of impact energy, E/u, compared to the present model. Data are He, circles; N, squares; Ar, triangles; and Xe, stars, from the same references as in Fig. 1.

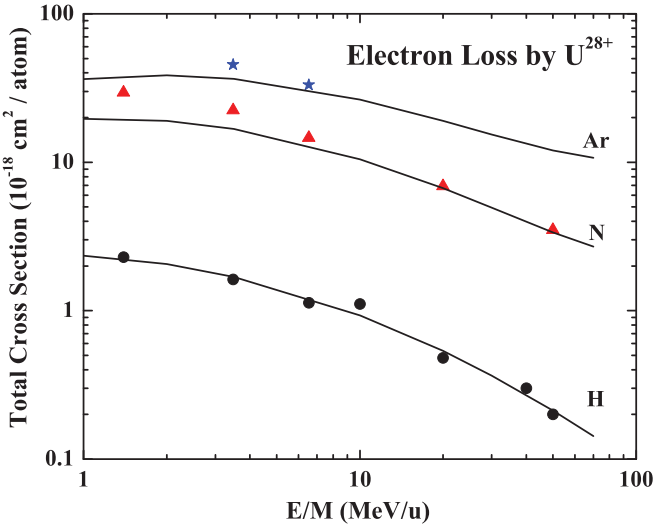

FIG. 5. (Color online) Total-electron-loss cross sections for U^{28+} ions colliding with H, N, and Ar atoms. The symbols are experimental data from Refs. [38,41,42]. The lines are scaled cross sections obtained using the present model and normalization to the experimental H data.

Figures 3–5 present comparisons of this model to available experimental data. In Figs. 3 and 4, the experimental data and our model results are normalized to unity for Ne targets. Figure 3 shows a comparison as a function of the target atomic number, Z_T, and Fig. 4 shows a comparison as a function of the collision energy E in MeV/u. In both cases, the experimental data are the same as in Fig. 1. The present model is seen to have the correct qualitative features, with the largest quantitative discrepancies with experiment occurring for the highest impact energies and heaviest targets. Although the original intent of this study was to address the target dependence question, our model also answers a second long-standing question with regard to electron loss at high energies, namely, why do light targets yield an E^{-1} cross-section dependence, whereas heavier targets yield a slower dependence on the order of v^{-1}. Figure 4 shows that the energy dependences of the normalized cross sections systematically increase as the target becomes heavier. This is because both $N_{T\mathrm{eff}}$ and $Z_{T\mathrm{eff}}$ are changing, in part because of relativistic effects and in part because of saturation effects. Thus, with respect to stripping by a Ne target, the cross sections for stripping by a light target such as hydrogen will decrease faster as a function of impact energy than they will for stripping by a heavier target.

Although our scaling formula was derived using cross sections for single-electron loss, Fig. 5 shows that it can also be applied to total loss cross sections. This is because, as stated earlier, the cross sections for single-electron loss and total electron loss showed very similar dependences as a function of Z_T and E. Figure 5 illustrates the quantitative predictability of the present model using measured total cross sections for electron loss by U^{28+} ions. Here, the experimental cross sections for a hydrogen target were multiplied by Eq. (18) to generate cross sections for stripping by nitrogen and argon targets. The procedure used was to first determine values for $\langle n_0 \rangle$ using Eq. (19). Next, Eq. (17) was used to determine $N_{T\mathrm{eff}}$ and the exponential saturation term was calculated using Eq. (18). Finally, scaling ratios with respect to H, e.g., N/H and Ar/H ratios, were calculated at each energy and multiplying by a curve fitted through the measured cross sections (divided by two) for an H_2 target to obtain absolute cross sections for interactions with N and Ar targets. Examples of the various values determined at 10 and 50 MeV/u are provided in Table I. For extrapolation to higher energies, it is suggested that the hydrogen cross sections be extended using an E^{-1} fit between 10 and 50 MeV/u and that these cross sections be multiplied by ratios determined from our model. Although not shown, in Fig. 5 such an extrapolation would yield cross sections that are approximately 10% larger at 100 MeV/u than those obtained by direct application of our model.

Figure 5 shows that the agreement using our model predictions is very good for energies above a few MeV/u. For comparison purposes, a Born scaling using the full nuclear charge for the antiscreening and screening terms would predict N and Ar cross sections that are too large by a factor of 4 and 12, respectively, in the few to tens of MeV/u range. More important is that a pure Born scaling would predict entirely different velocity dependences. This means that, even after division by the above factors in order to achieve reasonable agreement with experiment between 1 and 50 MeV/u, at 100 MeV/u a pure Born scaling would yield Ar and N values that are 3.5 and 1.5 times smaller than those predicted by our model. At higher energies, the deviation between a "pure Born" and our model will be even greater.

As a final note, our scaling model requires normalization to absolute cross sections. These can be obtained from experiment or theory and can be done for any atomic or molecular target. For extrapolation to higher energies, normalization to absolute H or He cross sections is best since, at high energies, these cross sections can be assumed to decrease as E^{-1}. Also note that the method just outlined provides projectile

TABLE I. Examples of quantities used to calculate the scaled cross sections for stripping of U^{28+} ions by H, N, and Ar atoms. Where two values are shown, they are for 10 and 50 MeV/u, respectively.

	H	N	Ar
$\langle n_0 \rangle$ [from Eq. (19)]	0.7	4.2	8.3
$N_{T\mathrm{eff}}$ [from Eq. (17)]	0.7 / 0.9	4.5 / 5.8	9.3 / 14
$Z_{T\mathrm{eff}}$ [from Eq. (15)]	0.5 / 0.5	2.8 / 4.2	5.8 / 9.5
Saturation factor ($e^{-Z_{T\mathrm{eff}}/v\ (\mathrm{in\ a.u.})}$)	0.98 / 0.99	0.87 / 0.91	0.76 / 0.80
Scaling factor [bracketed term in Eq. (18)]	0.94 / 1.27	10.6 / 20.2	26.7 / 71.9
Scaling factor ratio (with respect to H)	1.00 / 1.00	11.3 / 15.8	28.4 / 56.5

electron-loss cross sections per target atom. For molecular targets, the same procedure is used, but in calculating the scaling factor, the target nuclear charge Z_T is replaced by the average target nuclear charge per atom as suggested by Watson *et al*. [8]. Additionally, in the final conversion to cross sections, the scaling factor thus obtained is multiplied by the total number of atoms in the molecule.

V. SUMMARY

Electron-loss scaling as a function of the target was investigated using data taken from the literature. Strong similarities in the target Z dependences were found for a wide range of projectile species and for impact velocities ranging from some tens of eV/u to fractions of the speed of light. The comparison of the available scaling models with experiment showed that none provides a good fit of the data for a wide range of targets and collision energies. A model, based on a Born scaling and including both the antiscreening and screening contributions to projectile electron loss, was developed. It was found that, with the inclusion of relativistic effects which increase the contributions from both channels at high energies, and "target saturation" effects which reduce the contribution from the screening channel for heavy targets and lower impact energies, this modified Born model provides a reasonable fit to all available data. It was shown that this model is in qualitative agreement with the available data, independent of projectile species or charge state, impact energy, and target. Quantitatively, the maximum disagreement occurred at the highest energies and heaviest targets, being of ∼30%. One outcome of this model was the insight into why projectile stripping by light and heavy targets have different velocity dependences A simple formula which can be applied for both atomic and molecular targets and for impact energies ranging from a few to many tens of MeV/u or higher was provided.

ACKNOWLEDGMENTS

The National Science Foundation, the Fulbright Commission, the ExtreMe Matter Institute EMMI at the GSI Helmholzzentrum in Germany, and the Brazilian agencies CNPq and FAPERJ provided support for this work.

[1] C. Omet, P. Spiller, J. Stadlmann, and D. H. H. Hoffmann, New J. Phys. **8**, 284 (2006).
[2] See [accelconf.web.cern.ch/accelconf/l04/PAPERS/TUP27.PDF]
[3] See [www.rhichome.bnl.gov/RHIC/RAP/rhic_notes/AD-AP-1-51/AD-AP-42.pdf]
[4] FAIR Baseline Technical Report, 2006 [http://www.fair-center.de/Publikationen.171.0.html?&L=1]
[5] G. D. Alton, L. B. Bridwell, M. Lucas, C. D. Moak, P. D. Miller, C. M. Jones, Q. C. Kessel, A. A. Antar, and M. D. Brown, Phys. Rev. A **23**, 1073 (1981).
[6] G. M. Sigaud, F. S. Jorás, A. C. F. Santos, E. C. Montenegro, M. M. Sant'Anna, and W. S. Melo, Nucl. Instrum. Methods Phys. Res. B **132**, 312 (1997).
[7] A. C. F. Santos, G. M. Sigaud, W. S. Melo, M. M. Sant'Anna, and E. C. Montenegro, Phys. Rev. A **82**, 012704 (2010).
[8] R. L. Watson, Yong Peng, V. Horvat, G. J. Kim, and R. E. Olson, Phys. Rev. A **67**, 022706 (2003).
[9] D. Mueller, L. Grisham, I. Kaganovich, R. L. Watson, V. Horvat, K. E. Zaharakis, and M. S. Armel, Phys. Plasmas **8**, 1753 (2001).
[10] D. Mueller, L. Grisham, I. Kaganovich, R. L. Watson, V. Horvat, K. E. Zaharakis, and Y. Peng, Princeton Plasma Physics Laboratory Document No. PPPL-3713, 2002.
[11] R. D. DuBois *et al*., Phys. Rev. A **70**, 032712 (2004).
[12] H. Martínez, A. Amaya-Tapia, and J. M. Hernández, J. Phys. B **33**, 1935 (2000).
[13] H. Knudsen, C. D. Moak, C. M. Jones, P. D. Miller, R. O. Sayer, G. D. Alton, and L. B. Bridwell, Phys. Rev. A **19**, 1029 (1979).
[14] W. G. Graham, K. H. Berkner, R. V. Pyle, A. S. Schlachter, J. W. Stearns, and J. A. Tanis, Phys. Rev. A **30**, 722 (1984).
[15] N. Bohr, K. Dan. Vidensk. Selsk. Mat. Fys. Medd. **18**, No. 8 (1948).
[16] O. B. Firsov, Zh. Eksp. Teor. Fiz. **34**, 447 (1958) [JETP **7**, 308 (1958)].
[17] D. R. Bates and G. Griffing, Proc. Phys. Soc. A **68**, 90 (1955).
[18] R. Anholt, Phys. Lett. A **114**, 126 (1986).
[19] N. Stolterfoht, in *Spectroscopy and Collisions of Few-Electron Ions*, edited by M. Ivascu, V. Florescu, and V. Zoran (World Scientific, Singapore, 1989), p. 342.
[20] E. C. Montenegro, W. E. Meyerhof, and J. H. McGuire, Adv. At., Mol., Opt. Phys. **34**, 249 (1994).
[21] R. D. DuBois and S. T. Manson, Phys. Rev. A **42**, 1222 (1990).
[22] A. B. Voitkiv, G. M. Sigaud, and E. C. Montenegro, Phys. Rev. A **59**, 2794 (1999).
[23] M. M. Sant'Anna, W. S. Melo, A. C. F. Santos, G. M. Sigaud, E. C. Montenegro, M. B. Shah, and W. E. Meyerhof, Phys. Rev. A **58**, 1204 (1998).
[24] E. C. Montenegro, A. C. F. Santos, W. S. Melo, M. M. Sant'Anna, and G. M. Sigaud, Phys. Rev. Lett. **88**, 013201 (2002).
[25] E. C. Montenegro and T. J. M. Zouros, Phys. Rev. A **50**, 3186 (1994).
[26] A. C. F. Santos, G. M. Sigaud, W. S. Melo, M. M. Sant'Anna, and E. C. Montenegro, J. Phys. B **44**, 045202 (2011).
[27] W. E. Meyerhof, H.-P. Hüllskötter, Qiang Dai, J. H. McGuire, and Y. D. Wang, Phys. Rev. A **43**, 5907 (1991).
[28] E. C. Montenegro and W. E. Meyerhof, Phys. Rev. A **44**, 7229 (1991); **46**, 5506 (1992).
[29] M. M. Sant'Anna, W. S. Melo, A. C. F. Santos, G. M. Sigaud, and E. C. Montenegro, Nucl. Instrum. Methods Phys. Res. B **99**, 46 (1995).
[30] W. S. Melo, M. M. Sant'Anna, A. C. F. Santos, G. M. Sigaud, and E. C. Montenegro, Phys. Rev. A **60**, 1124 (1999).
[31] E. C. Montenegro and W. E. Meyerhof, Phys. Rev. A **43**, 2289 (1991).

[32] V. P. Shevelko, I. Yu Tolstikhina, and Th. Stöhlker, Nucl. Instrum. Methods Phys. Res. B **184**, 295 (2001).
[33] I. L. Beigman et al., Tech. Phys. **53**, 547 (2008).
[34] M.-Y. Song, M. S. Litsarev, V. P. Shevelko, H. Tawara and J.-S. Yoon, Nucl. Instrum. Methods Phys. Res. B **267**, 2369 (2009).
[35] T. Kaneko, Phys. Rev. A **32**, 2175 (1985).
[36] R. E. Olson, R. L. Watson, V. Horvat, and K. E. Zaharakis, J. Phys. B **35**, 1893 (2002).
[37] R. D. DuBois *et al.*, Phys. Rev. A **68**, 042701 (2003).
[38] R. E. Olson, R. L. Watson, V. Horvat, A. N. Perumal, Y. Peng, and Th. Stöhlker, J. Phys. B **37**, 4539 (2004).
[39] R. E. Olson, R. L. Watson, V. Horvat, K. E. Zaharakis, R. D. DuBois, and Th. Stöhlker, Nucl. Instrum. Methods Phys. Res. A **544**, 333 (2005).
[40] A. B. Voitkiv, B. Najjari, and V. P. Shevelko, Phys. Rev. A **82**, 022707 (2010).
[41] G. Weber *et al.*, Phys. Rev. ST Accel. Beams **12**, 084201 (2009).
[42] B. Franzke, IEEE Trans. Nucl. Sci. **28**, 2116 (1981).